Gut microbiome dysbiosis during COVID-19 is associated with increased risk for bacteremia and microbial translocation.

Mericien Venzon[*1,2], Lucie Bernard[*2], Jon Klein[*3], Jordan E. Axelrad[*4], Grant A. Hussey[5], Alexis P. Sullivan[5], Arnau Casanovas-Massana[6], Maria G. Noval[7], Ana M. Valero-Jimenez[7], Juan Gago[1,8], Evan Wilder[4], Yale IMPACT Research Team[11], Lorna E. Thorpe[8], Dan R. Littman[2,9], Meike Dittmann[7], Kenneth A. Stapleford[7], Bo Shopsin[10], Victor J. Torres[7], Albert I. Ko[6], Akiko Iwasaki[3,9], Ken Cadwell[2,4,7]†, Jonas Schluter[5,7]†

1. Vilcek Institute of Graduate Biomedical Sciences, New York University Grossman School of Medicine, New York, NY, USA
2. Kimmel Center for Biology and Medicine at the Skirball Institute, New York University Grossman School of Medicine, New York, NY, 10016, USA
3. Department of Immunobiology, Yale University School of Medicine, New Haven, CT, USA
4. Division of Gastroenterology, Department of Medicine, New York University Grossman School of Medicine, New York, NY, USA
5. Institute for Computational Medicine, New York University Grossman School of Medicine, New York, NY, USA
6. Department of Epidemiology of Microbial Diseases, Yale School of Public Health, New Haven, CT, USA.
7. Department of Microbiology, New York University Grossman School of Medicine, New York, NY, USA
8. Department of Population Health, New York University Grossman School of Medicine, New York, NY, USA.
9. Howard Hughes Medical Institute, Chevy Chase, MD.
10. Department of Medicine, Division of Infectious Diseases, New York University Grossman School of Medicine, New York, NY, USA
11. IMPACT team members listed in the appendix.

*) These authors contributed equally

Correspondence:

† ken.cadwell@nyulangone.org

† jonas.schluter@nyulangone.org

Abstract

The microbial populations in the gut microbiome have recently been associated with COVID-19 disease severity. However, a causal impact of the gut microbiome on COVID-19 patient health has not been established. Here we provide evidence that gut microbiome dysbiosis is associated with translocation of bacteria into the blood during COVID-19, causing life-threatening secondary infections. Antibiotics and other treatments during COVID-19 can potentially confound microbiome associations. We therefore first demonstrate that the gut microbiome is directly affected by SARS-CoV-2 infection in a dose-dependent manner in a mouse model, causally linking viral infection and gut microbiome dysbiosis. Comparison with stool samples collected from 101 COVID-19 patients at two different clinical sites also revealed substantial gut microbiome dysbiosis, paralleling our observations in the animal model. Specifically, we observed blooms of opportunistic pathogenic bacterial genera known to include antimicrobial-resistant species in hospitalized COVID-19 patients. Analysis of blood culture results testing for secondary microbial bloodstream infections with paired microbiome data obtained from these patients suggest that bacteria translocate from the gut into the systemic circulation of COVID-19 patients. These results are consistent with a direct role for gut microbiome dysbiosis in enabling dangerous secondary infections during COVID-19.

50 **Main text**

51 A better understanding of factors contributing to the pathology of coronavirus disease 2019 (COVID-19) is
52 an urgent global priority. Infections by SARS-CoV-2 are frequently asymptomatic or mild in nature, but
53 may also cause a broad range of severe and life-threatening symptoms. Previous reports have
54 demonstrated that severe COVID-19 is frequently associated with specific inflammatory immune
55 phenotypes, lymphopenia, and a generally disproportionate immune response leading to systemic organ
56 failure[1,2]. Even in mild cases, gastrointestinal symptoms are reported frequently, and recent studies
57 reported that COVID-19 patients lose commensal taxa of the gut microbiome during hospitalization[3,4].
58 Differences in gut bacterial populations relative to healthy controls were observed in all COVID-19
59 patients, but most strongly in patients who were treated with antibiotics during their hospitalization[4]. Most
60 recently, COVID-19 patients treated with broad spectrum antibiotics at admission were shown to have
61 increased susceptibility to multi-drug resistant infections and nearly double the mortality rate from septic
62 shock[5,6], and a recent meta-analysis found that over 14% of 3,338 COVID-19 patients acquired a
63 secondary bacterial infection[7]. However, the causal direction of the relationship between disease
64 symptoms and gut bacterial populations is not yet clear.

65 Complex gut microbiota ecosystems can prevent the invasion of potentially pathogenic
66 bacteria[8,9]. Conversely, when the gut microbiota incurs damage, such as through antibiotics treatment,
67 competitive exclusion of pathogens is weakened[10] and potentially dangerous blooms of antibiotic resistant
68 bacterial strains can occur [11,12]. In immunocompromised cancer patients, blooms of Enterococcaceae and
69 Gram-negative proteobacteria can lead to gut dominations by few or single species[13–16]. Gut domination
70 events are dangerous to these patients because antibiotic resistant bacteria may translocate from the gut
71 into the blood stream. Consequently, enterococcal dominations have been associated with 9-fold
72 increased risk of bloodstream infections (BSIs) with vancomycin-resistant Enterococcus (VRE), and
73 domination by Gram-negative proteobacteria with 5-fold increased risk of Gram-negative rod BSIs[13].
74 Bacterial co-infection can also cause life-threatening complications in patients with severe viral
75 infections[6,17]; therefore, antibacterial agents were administered empirically to nearly all critically ill
76 suspected COVID-19 patients since the incidence of bacterial superinfection was unknown early during
77 the pandemic[4,18]. However, it is now known that nosocomial infection during prolonged hospitalization is
78 the primary threat to patients with COVID-19[19], rather than bacterial co-infection upon hospital
79 admission[7,20–22]. Evidence from immunocompromised cancer patients suggests that indiscriminate
80 administration of broad-spectrum antibiotics may, counter-intuitively, increase nosocomial BSI rates by
81 causing gut dominations of resistant microbes that can translocate into the blood[13,23]. Thus, empiric
82 antimicrobial use, i.e. without direct evidence for a bacterial infection, in patients with severe COVID-19
83 may be especially pernicious because it may select for antimicrobial resistance and could promote gut
84 translocation-associated BSI.

85

The role of the gut microbiome in respiratory viral infections in general[24], and in COVID-19 patients in particular, is only beginning to be understood. Animal models of influenza virus infection have uncovered mechanisms by which the microbiome influences antiviral immunity[25–27], and in turn, the viral infection was shown to disrupt the intestinal barrier of mice by damaging the gut microbiota[28,29]. Hence, we hypothesized that gut dysbiosis during COVID-19 may be associated with BSIs. To test this, we first determined whether SARS-CoV-2 infection could directly cause gut dysbiosis independently of hospitalization and treatment. Daily changes in fecal bacterial populations were monitored following intranasal inoculation of transgenic mice expressing human *ACE2* driven by the *cytokeratin-18* promoter (*K18-ACE2tg* mice) with either a high dose (HD,10^4PFU) or low dose (LD, 10PFU) of SARS-CoV-2 (**Figure 1a**). Although disease was not as evident in LD mice, we confirmed the presence of infectious virus in the lung by plaque assay at sacrifice (**Extended Data Figure S1**). Among the HD mice, we observed significant microbiome changes (**Figure 1b**), with a repeatedly observed community trajectory corresponding to a loss in relative abundances of obligate anaerobe species such as members of the Clostridiales order (**Figure 1c**), concurrent with an expansion of Verrucomicrobiales (**Figure 1a,c**). During this shift in the microbiome, α-diversity in the gut bacterial ecosystem was decreasing, a trend also observed in the LD mice, albeit to a lesser extent, but not in the control mice (**Figure 1b**). After less than one week of viral infection, α-diversity was reduced in infected mice (**Figure 1b**, 95%HDI<0 Bayesian estimation of differences in group means BEST, methods). Alongside the progressive increase in microbiota compositional dysbiosis, we also observed systemic signs of severe infection, including weight loss (**Extended Data Figure S2**), as well as ruffled fur, heavy breathing, reduced activity and hunched posture (**Extended Data Table S1**). These results demonstrate that SARS-CoV2 infection directly causes gut microbiome dysbiosis in a mouse model.

We next profiled the bacterial composition of the fecal microbiome in 138 samples (**Figure 2a**) obtained from SARS-CoV-2 infected patients treated at NYU Langone Health (NYU, 73 samples, **Extended Data Table S2**) and Yale New Haven Hospital (YALE, 65 samples, **Extended Data Table S3**). Analysis of metagenomic data obtained from sequencing of the 16S rRNA genes revealed a wide range of bacterial community diversities, as measured by the inverse Simpson index, in samples from both centers (NYU: [1.0, 32.2], YALE: [1.5, 29.3], **Figure 2b**); on average, samples from NYU were less diverse (-2.5, $p<0.01$, **Figure 2c**). However, the composition in samples between the two centers did not show systematic compositional differences (**Figure 2d,e,f**). On average, in both centers, members of the phyla Firmicutes and Bacteroidetes represented the most abundant bacteria, followed by Proteobacteria (**Figure 2d**). The wide range of bacterial diversities was reflected in the high variability of bacterial compositions across samples (**Figure 2e,f**). In samples from both centers, microbiome dominations, defined as a community where a single genus reached more than 50% of the population, were observed frequently (NYU: 21 samples, YALE: 12 samples), representing states of severe microbiome injury in COVID-19 patients (**Figure 2g**).

In agreement with a recent study associating gut microbial compositions with disease severity[4], we found that samples from patients who were treated in the ICU had reduced bacterial diversity (**Extended Data Figure S3a**). In 22 cases, gastrointestinal symptoms were recorded, but only two of those patients required ICU treatment and corresponding stool samples had higher average diversity than other samples (**Extended Data Figure S3b**,**d**). Strikingly, however, samples associated with a BSI had strongly reduced bacterial α-diversities (mean difference: -7.7, CI_{BEST}[-10.2, -5.2], **Extended Data Figure S3c**).

The lower diversity associated with samples from 21 patients with BSIs led us to investigate their bacterial taxon compositions and the potential that gut dysbiosis was associated with BSI events. All BSI patients had received antibiotic treatments during hospitalization, which could exacerbate COVID-19 induced shifts in microbiota populations[11,12,15], but may indeed be administered in response to a suspected or confirmed BSI. However, we noted that most BSI patients (80%) also received antibiotics prior to their BSI. Principal coordinate analysis of all stool samples indicated that the BSI-associated samples spanned a broad range of compositions (**Figure 3a**). To identify bacterial abundance patterns that consistently distinguished BSI from non-BSI-associated samples, we next performed a Bayesian logistic regression. This analysis estimated the association of the 10 most abundant bacterial genera with BSI cases, i.e. it identified enrichment or depletion of bacterial genera in BSI associated samples (**Figure 3b**). This analysis revealed that the genus *Faecalibacterium* was negatively associated with BSI (OR: -1.49, CI:[-2.82, -0.18]). *Faecalibacterium* is an immunosupportive Clostridiales genus that is a prominent member of the human gut microbiome[30–32], and its reduction is associated with disruption to intestinal barrier function[33,34], perhaps via ecological network effects[34].

To evaluate the effect size of the association between *Faecalibacterium* and BSIs, we performed a posterior predictive check. Using the average genus composition found across all samples, we first computed the distribution of predicted BSI risks (**Figure 3c**), and compared this risk distribution with a hypothetical bacterial composition which increased *Faecalibacterium* by 10% points. The predicted risk distributions associated with these two compositions differed strongly (mean difference 26%, CI: [-9%, 67%], **Figure 3c**). Domination states of the microbiome increase the risk for BSIs in immunocompromised cancer patients [13]; such dominations imply high relative abundances of single taxa, and therefore a low diversity. Consistent with this, *Faecalibacterium* abundance was positively correlated with diversity (R: 0.55, $p<10^{-10}$, **Figure 3d**) in our data set and as reported previously [30].

We therefore next investigated a direct association between the bacteria populating the gut microbiome and the organisms identified in the blood of patients. Visualizing the bacterial composition in stool samples from patients alongside the BSI microorganism (**Extended Data Figure S4**, **Figure 3e**) suggested a correspondence with the respective taxa identified in the blood: high abundances of the BSI-causing microbes were found in corresponding stool samples (**Figure 3e**). To analyze this, we first assigned stool samples associated with each BSI event into 5 categories defined by the taxonomic order of the causative bacterial organisms, as well as one singleton group of a fungal infection case as a sixth

159 category; stool samples from uninfected patients were assigned a seventh, “uninfected” category. For
160 samples of each BSI category, we first calculated their median abundances of bacterial predictors in the
161 stool. We then ranked these stool taxon median abundances across BSI categories. As expected from
162 the visualization of sample compositions (**Figure 3e**), we found that BSI category sample sets were
163 generally enriched in their respective taxa in the stool. For example, samples associated with *Klebsiella*,
164 *Escherichia* or *Serratia* BSIs (Enbct category, **Figure 3f**) had the highest rank of Enterobacterales
165 abundances across the BSI category sample sets (**Figure 3f**). We tested this observation statistically
166 using the $\log_{10}$-relative bacterial abundances in stool samples as independent predictors of identified BSI
167 pathogens, i.e. the BSI category, in a Bayesian categorical regression model where the uninfected class
168 was used as a pivot (see methods). In addition to taxon abundances, the model included the bacterial
169 α-diversity as a predictor. As expected, a strong statistical association between diversity and BSIs in
170 general was detected (**Extended Data Figure S5**). The rank analysis had suggested that
171 Staphylococcales are not enriched in BSIs by *Staphylococcus* (**Figure 3f**); this was supported by the
172 Bayesian model which showed that $\log_{10}$-abundances of Staphylococcales in the stool were not
173 detectably predictive of a *Staphylococcus* BSI. By contrast, our analysis demonstrated that the bacterial
174 abundances of all other BSI-causing organisms in the stool were predictive of corresponding BSIs.
175 Collectively, these results reveal an unappreciated link between SARS-CoV-2 infection, gut
176 microbiome dysbiosis, and a major complication of COVID-19, BSIs. The loss of diversity and
177 immunosupportive *Faecalibacterium* in patients with BSIs mirrored a similar loss of diversity and
178 Clostridiales in the mice receiving high doses of SARS-CoV-2, suggesting that this virus causally affects
179 the microbiome, either through direct infection[35–39] or through a systemic inflammatory response [2,4].
180 However, the dysbiosis in patients with COVID-19 exceeded the microbiota shifts observed in the mouse
181 experiments, including microbiome dominations by single taxa, which was not seen in the mouse
182 experiments. It is possible that in our experiment, mice were sacrificed before perturbations to the gut
183 microbial populations reached a maximum. However, it is also plausible that the frequently administered
184 antibiotic treatments that hospitalized COVID-19 patients receive exacerbated SARS-CoV-2 induced
185 microbiome perturbations. Additionally, unlike the controlled environment experienced by laboratory mice,
186 hospitalized patients are uniquely exposed to antimicrobial-resistant infectious agents present on
187 surfaces and shed by other patients. Indeed, domination events where the gut is populated by only a few
188 taxa have been described in hospitalized, immunocompromised cancer patients treated with broad
189 spectrum antibiotics[15]. We frequently observed such dominations in our COVID-19 cohorts treated at two
190 hospitals.
191 Our observation that the type of bacteria that entered the bloodstream was disproportionately
192 enriched in the associated stool samples is a well characterized phenomenon in cancer patients[13],
193 especially during chemotherapy induced leukocytopenia when patients are severely
194 immunocompromised[11,30]. COVID-19 patients are also immunocompromised and frequently incur
195 lymphopenia, rendering them susceptible to secondary infections[40]. Our data suggests dynamics in

196 COVID-19 patients may be similar to those observed in cancer patients: BSI-causing organisms may
197 translocate from the gut into the blood, potentially due to loss of gut barrier integrity, through virus-
198 induced tissue damage rather than chemotherapy. Consistent with this possibility, soluble immune
199 mediators such as TNFa and interferons produced during viral infections, including SARS-CoV-2,
200 damage the intestinal epithelium to disrupt the gut barrier, especially when the inflammatory response is
201 sustained as observed in patient with severe COVID-19[41–43].
202 One limitation of our data is temporal ordering of samples. Occasionally stool samples were
203 collected after observation of BSI, and this mismatch in temporal ordering is counter intuitive for gut-to-
204 blood translocation and a causal interpretation of our associations. However, the reverse direction, that
205 blood infection populates and changes the gut community, is unlikely for the organisms identified in the
206 blood, and if our associations were not causal, we would expect no match between BSI organisms and
207 stool compositions.
208 Taken together, our findings support a scenario in which gut-to-blood translocation of
209 microorganisms following microbiome dysbiosis, a known issue for chronic conditions such as cancer,
210 leads to dangerous BSIs during COVID-19. We suggest that investigating the underlying mechanism
211 behind our observations will inform the judicious application of antibiotics and immunosuppressives in
212 patients with respiratory viral infections and increase our resilience to pandemics.
213
214 **Materials and Methods**
215 *Bioethics statement*
216 The collection of COVID-19 human biospecimens for research has been approved by the NYUSOM
217 Institutional Review Board under il8-01121 Inflammatory Bowel Disease and Enteric Infection at NYU
218 Langone Health. The data presented in this study were also approved by Yale Human Research
219 Protection Program Institutional Review Boards (FWA00002571, protocol ID 2000027690). Informed
220 consent was obtained from all enrolled patients.
221
222 *Mouse experiments*
223 <u>Cells & virus</u>
224 Vero E6 (CRL-1586; American Type Culture Collection) were cultured Dulbecco's Modified Eagle's
225 Medium (DMEM,Corning) supplemented with 10% fetal bovine serum (FBS, Atlanta Biologics) and 1%
226 nonessential amino acids (NEAA,Corning). SARS-CoV-2, isolate USA-WA1/2020 19 (BEI resources
227 #NR52281), a gift from Dr. Mark Mulligan at the NYU Langone Vaccine Center was amplified once in
228 Vero E6cells. All experiments with SARS-CoV-2 were conducted in the NYU Grossman School of
229 Medicine ABSL3 facility by personnel equipped with powered air-purifying respirators.
230
231 <u>Mice</u>
232 Heterozygous K18-hACE2 C57BL/6J mice (strain: 2B6.Cg-Tg(K18-ACE2)2Prlmn/J) were obtained from

233 The Jackson Laboratory. Animals were housed in groups and fed standard chow diets. All animal studies
234 were performed according to protocols approved by the NYU School of Medicine Institutional Animal Care
235 and Use Committee (IACUC n°170209). 24-week-old K18-hACE2 males were administered either 10PFU
236 SARS-CoV-2 (low dose, LD), 10^4PFU SARS-CoV-2 (high dose, HD) diluted in 50µL PBS (Corning) or
237 50µL PBS (non-infected, CTRL) via intranasal administration under xylazine-ketamine anesthesia
238 (AnaSedR AKORN Animal Health, KetathesiaTM Henry Schein Inc). Viral titer in the inoculum was
239 verified by plaque assay in Vero E6 cells. Following infection, mice were monitored daily for weight loss
240 and signs of disease. Stool samples were collected and stored at -80°C.
241
242 Measurement of viral load by plaque assay
243 Six or seven days after infection, mice were sacrificed. For some mice lungs were collected in Eppendorf
244 tubes containing 500µl of PBS and a 5mm stainless steel bead (Qiagen) and homogenized using with the
245 Qiagen TissueLyser II. Homogenates were cleared for 5 min at 5,000 × g, and viral supernatant was
246 frozen at -80°C for titration through plaque assay. In brief, Vero E6 cells were seeded at a density of 2.2 ∗
247 10^5 cells per well in flat-bottom 24-well tissue culture plates. The following day, media was removed and
248 replaced with 100µL of tenfold serial dilutions of the virus stock, diluted in infection medium. Plates were
249 incubated for 1h at 37°C. Following incubation, cells were overlaid with 0.8% agarose in DMEM
250 containing 2% FBS and incubated at 37°C for 72hrs. Cells were then fixed with formalin buffered 10%
251 (Fisher Chemical) for 1h. Agarose plugs were then removed and cells were stained for 20 min with crystal
252 violet and then washed with tap water.
253
254 *Human study population and data collection*
255 This study involved 101 patients with laboratory-confirmed SARS-CoV-2 infection. SARS-CoV-2 infection
256 was confirmed by a positive result of real-time reverse transcriptase-polymerase chain reaction assay on
257 a nasopharyngeal swab. 64 patients were seen at NYU Langone Health, New York, for routine medical
258 procedures, outpatient care, or admitted through the Emergency Department at NYU Langone Health's
259 Tisch Hospital, New York City, between January 29, 2020 – July 2, 2020 and were followed until
260 discharge. In order to be eligible for inclusion in the study, stool specimens needed to be from individuals
261 >18 years of age. Data including demographic information, clinical outcomes, and laboratory results were
262 extracted from the electronic medical records in the NYU Langone Health clinical management system.
263 Blood and stool samples were collected by hospital staff. OmnigeneGut kits were used on collected stool.
264 In parallel, 37 patients were admitted to YNHH with COVID-19 between 18 March 2020 and 27 May 2020
265 as part of the YALE IMPACT cohort described at length elsewhere[2]. Briefly, participants were enrolled
266 after providing informed consent and paired blood and stool samples were collected longitudinally where
267 feasible for duration of hospital admission. No statistical methods were used to predetermine sample size
268 for this cohort. Demographic information of patients was aggregated through a systematic and
269 retrospective review of the EHR and was used to construct **Extended Data Table 3**. Symptom onset and

aetiology were recorded through standardized interviews with patients or patient surrogates upon enrolment in our study, or alternatively through manual EHR review if no interview was possible owing to clinical status at enrolment. The clinical data were collected using EPIC EHR and REDCap 9.3.6 software. At the time of sample acquisition and processing, investigators were blinded to patient clinical status.

DNA extraction and bacterial 16S rRNA sequencing

For bacterial DNA extraction 700µL of SL1 lysis buffer (NucleoSpin Soil kit, Macherey-Nagel) was added to the stool samples and tubes were heated at 95°C for 2h to inactivate SARS-CoV-2. Samples were then homogenized using the FastPrep-24TM instrument (MP Biomedicals) and extraction was pursued using the NucleoSpin Soil kit according to the manufacturer's instructions. DNA concentration was assessed using a NanoDrop spectrophotometer. Samples with too low DNA concentration were excluded. DNA from human samples was extracted with PowerSoil Pro (Qiagen) on the QiaCube HT (Qiagen), using Powerbead Pro (Qiagen) plates with 0.5mm and 0.1mm ceramic beads. For mouse samples, the variable region 4 (V4) of the 16S rRNA gene was amplified by PCR using primers containing adapters for MiSeq sequencing and single-index barcodes. All PCR products were analyzed with the Agilent TapeStation for quality control and then pooled equimolar and sequenced directly in the Illumina MiSeq platform using the 2x250 bp protocol. Human samples were prepared with a protocol derived from [44], using KAPA HiFi Polymerase to amplify the V4 region of the 16S rRNA gene. Libraries were sequenced on an Illumina MiSeq using paired-end 2x250 reads and the MiSeq Reagent Kitv2.

Bioinformatic processing and taxonomic assignment

Amplicon sequence variants (ASVs) were generated via dada2 v1.16.0 using post-QC FASTQ files. Within the workflow, the paired FASTQ reads were trimmed, and then filtered to remove reads containing Ns, or with maximum expected errors >= 2. The dada2 learn error rate model was used to estimate the error profile prior to using the core dada2 algorithm for inferring the sample composition. Forward and reverse reads were merged by overlapping sequence, and chimeras were removed before taxonomic assignment. ASV taxonomy was assigned up to genus level using the SILVAv.138 database with the method described in [45] and a minimum boostrapping support of 50%. Species-level taxonomy was assigned to ASVs only with 100% identity and unambiguous matching to the reference.

Compositional analyses

<u>α-Diversity</u>

We calculated the inverse Simpson (*IVS*) index from relative ASV abundances (*p*) with *N* ASVs in a given sample, $IVS = \frac{1}{\sum_i^N p_i^2}$.

Principal Coordinate Analyses

Bray-Curtis distances were calculated from the filtered ASV table using QIIME 1.9.1 and principal components of the resulting distance matrix were calculated using the scikit-learn package for the Python programming language, used to embed sample compositions in the first two principal coordinates (see published code for the implementation in the Python programming language).

Average compositions and manipulation of compositions

To describe the average composition of a set of samples we calculated the central tendency of a compositional sample [46]. For counter factual statistical analyses that require changes to a composition, e.g. an increase in a specific taxon, we deployed the perturbation operation ($\oplus$), which is the compositional analogue to addition in Euclidean space[46]. A sample *x* containing the original relative taxon abundances is perturbed by a vector *y*,

$$y\colon\ x \oplus y = \left[\frac{x_1 y_1}{\sum_{i=1}^{D} x_i y_i}, \frac{x_2 y_2}{\sum_{i=1}^{D} x_i y_i}, \ldots, \frac{x_D y_D}{\sum_{i=1}^{D} x_i y_i}\right] \forall x, y \in S^D$$

where S^D represents the D-part simplex.

Statistical analyses

Computer code alongside processed data tables are made available and can be used to reproduce the statistical analysis and regenerate the figures (**Extended Data File 1**).

Bayesian ttest

To compare diversity measurements between different sample groups, e.g. different clinical status, we performed a Bayesian estimation of group differences (BEST, [47]) , implemented using the pymc3 package for the Python programming language; with priors (~) and deterministic calculations (=) to assess differences in estimated group means as follows:

$g_1 \sim \text{Normal}(\mu = 15, \sigma = 15)$

$g_2 \sim \text{Normal}(\mu = 15, \sigma = 15)$

$\sigma_{g1} \sim \text{Uniform}(\text{low} = 1e{-}4, \text{high} = 30)$

$\sigma_{g2} \sim \text{Uniform}(\text{low} = 1e{-}4, \text{high} = 30)$

$\nu \sim \text{Exponential}(1/15) + 1$

$\lambda_1 = \sigma_{g1}^{-2}$

$\lambda_2 = \sigma_{g2}^{-2}$

$G1 \sim \text{StudentT}(\text{nu} = \nu, \text{mu} = g_1, \text{lam} = \lambda_1)$

$G2 \sim \text{StudentT}(\text{nu} = \nu, \text{mu} = g_2, \text{lam} = \lambda_2)$

$\Delta = G1 - G2$

Bayesian inference was performed using “No U-turn sampling”[48]. Highest density intervals (HDI) of the posterior estimation of group differences (Δ) were used to determine statistical certainty (***: 99% HDI >0

342 or <0, **: 95%HDI, *:90% HDI). The BEST code is provided in the Extended Data and implemented
343 following the pymc3 documentation (**Extended Data File 1**).
344
345 Bayesian logistic regression
346 We performed a Bayesian logistic regression to distinguish compositional differences between infection-
347 associated samples and samples from patients without secondary infections. We modeled the infection
348 state of patient sample *i*, *yi* with a Binomial likelihood:

349 $$y_i \sim \text{Binomial}(n = 1, p = p)$$
350 $$p = \text{inverse logistic}(\alpha + X_i\beta)$$
351 $$\alpha \sim \text{Normal}(\mu = 0, \sigma = 1)$$
352 $$\beta \sim \text{Normal}(\mu = 0, \sigma = 1)$$

353 Where prior distributions are indicated by ~; α is the intercept of the generalized linear model, β is the
354 coefficient vector for the $\log_{10}$-relative taxon abundances X_i in sample *i*.
355
356 Bayesian categorical regression
357 To interrogate a correspondence between the taxon abundances in stool samples and the
358 microorganisms causing BSIs, we performed a Bayesian categorical regression. Briefly, we chose to
359 investigate an association between stool taxon abundances (independent predictor variable) and the
360 microbe identified in the blood (categorical outcome variable with seven unordered values) using a
361 multiclass regression (categorical regression). We estimated for each sample a probability of being
362 associated with one of the 6 BSI types (i.e. BSI by: Bacteroidaceae, Enterobacteriaceae,
363 Lactobacillaceae, Pseudomonadaceae, Staphylococcaceae, Saccharomycetaceae), and we used a
364 seventh class, uninfected, as a pivot. This means we are estimating a seven component simplical vector
365 (*s*) containing the probabilities of a sample to be associated with one of the seven categories (6 BSI types
366 and uninfected). For each category, we set up a linear model (s_g, where $_g$ indicates the category). Each
367 linear model includes $\log_{10}$-relative stool taxon abundances of the taxa corresponding to the BSI category.
368 Furthermore, we had shown that alpha diversity (IVS) was globally associated with BSI; thus, diversity
369 was a predictor in each linear model. We set up a model using varying intercept and varying slope terms
370 such that the linear models used partially pooled coefficients for baseline risks (β[1]) and slopes
371 corresponding to the stool sample predictors (β[2]). The multiclass probabilities in *s* were then obtained
372 by applying the softmax function. The following model and priors were used:

373 $$y_i \sim \text{Categorical}(p = p)$$
374 $$p = \text{softmax}(s)$$
375 $$z = (\sigma p * Lp) * zp$$
376 $$s_{Bacteroidaceae} = \beta[1] + z[1,1] + (\beta[2] + z[2,1]) * X_{Bacteroidaceae} + \beta_{diversity} * IVS$$
377 $$s_{Enterobacteriaceae} = \beta[1] + z[1,2] + (\beta[2] + z[2,2]) * X_{Enterobacteriaceae} + \beta_{diversity} * IVS$$
378 $$s_{Lactobacillaceae} = \beta[1] + z[1,3] + (\beta[2] + z[2,3]) * X_{Lactobacillaceae} + \beta_{diversity} * IVS$$

$$s_{Pseudomonadaceae} = \beta[1] + z[1,4] + (\beta[2] + z[2,4]) * X_{Pseudomonadaceae} + \beta_{diversity} * IVS$$

$$s_{Staphylococcaceae} = \alpha_{Staphylococcaceae} + \beta_{Staphylococcaceae} * X_{Staphylococcaceae} + \beta_{diversity} * IVS$$

$$s_{Saccharomycetaceae} = \alpha_{Saccharomycetaceae} + \beta_{diversity} * IVS$$

$$s_{uninfected} = 0$$

$$\beta \sim Normal(\mu = 0, \sigma = 1)$$

$$\sigma \sim Exponential(\lambda = 1)$$

$$\sigma p \sim Exponential(\lambda = 1)$$

$$Lp \sim LKJ\_corr\_choleski(2)$$

$$\alpha_{Staphylococcaceae} \sim Normal(\mu = 0, \sigma = 1)$$

$$\beta_{Staphylococcaceae} \sim Normal(\mu = 0, \sigma = 1)$$

$$\beta_{diversity} \sim Normal(\mu = 0, \sigma = 1)$$

$$\alpha_{Saccharomycetaceae} \sim Normal(\mu = 0, \sigma = 2)$$

$$zp \sim Normal(\mu = 0, \sigma = 1)$$

Where p corresponds to the probabilities of each category, β is a two-component variable for the intercept and slope terms, representing the global baseline probability of bacterial infections with Bacteroidaceae, Enterobacteriaceae, Lactobacillaceae, and Pseudomonadaceae as well as the global slope coefficient for the effect of stool $\log_{10}$-relative abundances, which are partially pooling information across bacterial infection categories. To achieve partial pooling and account for correlations between varying intercepts and slopes (z), we jointly inferred the Choleski-factorized covariance matrix (σp, Lp, zp), using the Lewandowski-Kurowicka-Joe (LKJ) distribution as a prior (LKJ_corr_choleski). $\beta_{diversity}$ is the coefficient for the effect of the *IVS* diversity. Of note, 16S rRNA sequencing does not provide abundances for the fungal infection by Saccharomycetaceae; therefore, we used only a baseline risk for this infection type ($\alpha_{Saccharomycetaceae}$) and IVS as predictors. To ensure equal prior probabilities for this category relative to the other categories, which have an additional predictor term and thus wider prior probabilities, we compensated the otherwise reduced prior uncertainty by widening the prior for $\alpha_{Saccharomycetaceae}$. Also, we assumed that infections by Staphylococcaceae could sometimes include contaminations from the skin of the patient or staff; therefore, we did not pool estimates for BSIs by Staphylococcaceae with other coefficients. The model was implemented in the STAN programming language and compiled using cmdstan. Code, the compiled STAN model, R notebooks to obtain and process the posterior chains, and data tables are provided in the supplement (**Extended Data File 2**).

411 **Data Availability**

412 All data is made available as Extended Data. We provide code and data to reproduce the main analyses
413 in the form of jupyter notebooks and R notebooks, alongside processed “tidy” data tables, compiled STAN
414 programs and code to regenerate the figures. The raw sequencing data have been deposited on the
415 Sequencing Reads Archive (SRA), and SRA accession numbers are available for two bioprojects
416 corresponding to the mouse sequencing data (**Extended Data File 3**) and the human stool samples
417 (**Extended Data File 4**).

418 **Figures and captions**

419 **Figure 1. SARS-CoV-2 infection causes gut microbiome alterations in mice**. **a** Time lines of fecal
420 microbiota composition measured by 16S rRNA gene sequencing in mice infected with high (HD, 10^4PFU),
421 or low doses (LD, 10PFU) and in uninfected control mice (CTRL); time of infection=Day 1. Bars represent
422 the composition of the 30 most abundant bacterial families per sample, blocks of samples correspond to
423 an individual mouse's time course. **b** *α*-diversity (Shannon) in the final samples per infection group; **:
424 HDI95<0 BEST. **c** log_{10}-relative family abundances at the final time point. heavy breathing, reduced activity
425 and hatched posture (Extended Data Table S1).

426 **Figure 2. Gut microbiome bacterial compositions during COVID-19 in patients from NYU Langone**
427 **Health and Yale New Haven Hospital**. **a** Bacterial family composition in stool samples identified by 16S
428 rRNA gene sequencing; bars represent the relative abundances of bacterial families; red circles indicate
429 samples with single taxa >50%. Samples are sorted by the bacterial *α*-diversity (inverse Simpson index,
430 **b**). **c** *α*-diversity in samples from NYU Langone Health and Yale New Haven Hospital. **d** Average phylum
431 level composition per center. **e-g** Principal coordinate plots of all samples shown in **a**, labeled by center
432 (**e**), most abundant bacterial family (**f**) and domination status of the sample (**g**).
433
434

435 **Figure 3. Microbiome composition is associated with secondary bloodstream infections**. **a** Principal
436 coordinate plot of all samples, BSI associated samples in orange. **b** Posterior coefficient estimates from a
437 Bayesian logistic regression regressing log_{10} relative abundances of the top 10 most abundant bacterial
438 genera on BSI status. **c** Posterior prediction of BSI risk based on bacterial composition contrasting the
439 predicted risk of the average composition across all samples (red) with the risk estimated for the same
440 composition changed such that *Faecalibacterium* was increased by 10% (blue). **d** Log_{10} relative
441 abundances of *Faecalibacterium* correlated with *α*-diversity, shaded region: 95%CI. **e** Sample
442 compositions with BSIs indicated; left: *Staphylococcus* BSI associated samples; right: other BSI associated
443 samples, the BSI causing microbial genus annotated in colors corresponding to the colors in stool
444 microbiome compositions. **f** Rank analysis of abundance patterns in stool samples from different BSI
445 categories; a filled circle indicates the calculated rank of the focal BSI category (row) in terms of the
446 corresponding taxon stool abundance relative to samples from other BSI categories (only 5 out of 7 BSI
447 categories are shown because fungal BSIs and the uninfected category have no corresponding bacterial
448 stool abundances). **g** Posterior coefficients of the statistical association between bacterial order log_{10}
449 relative abundances of BSI causing bacteria and BSI events from a hierarchical Bayesian categorical
450 regression; **: 95%HDI>0, *: 90%HDI>0, .:85% HDI>0.
451

452

Figure 1

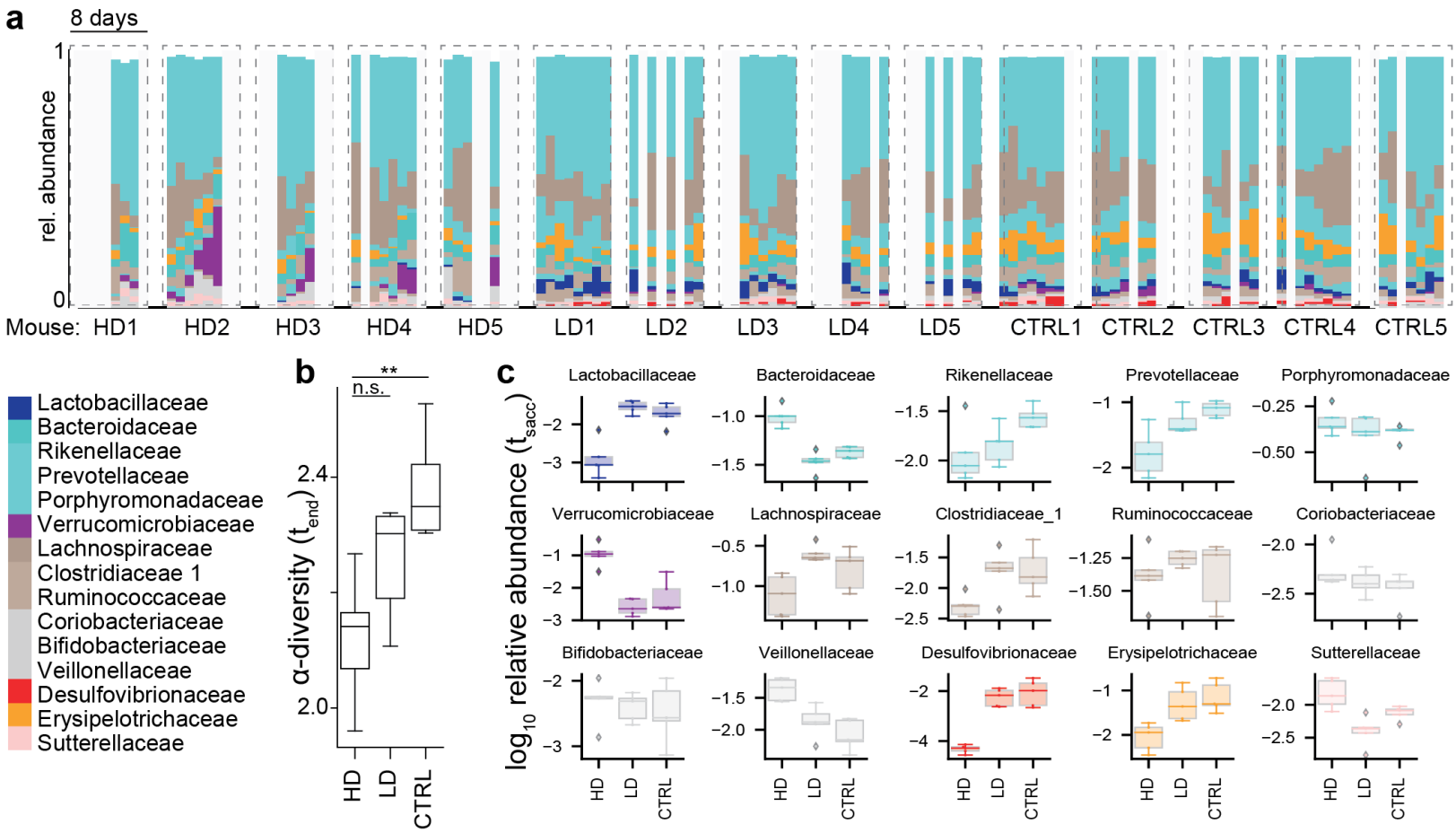

453
454

Figure 2

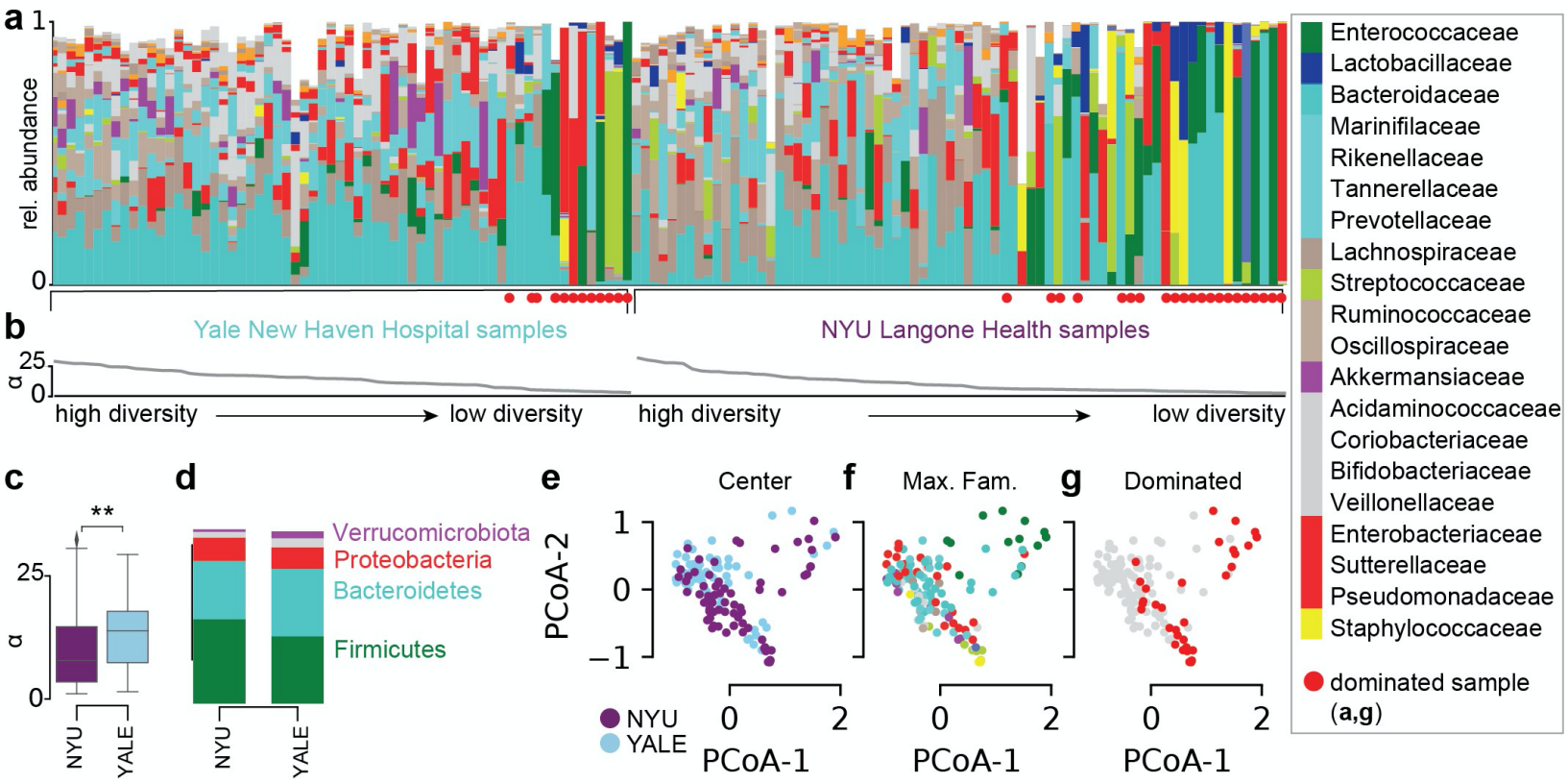

455
456
457

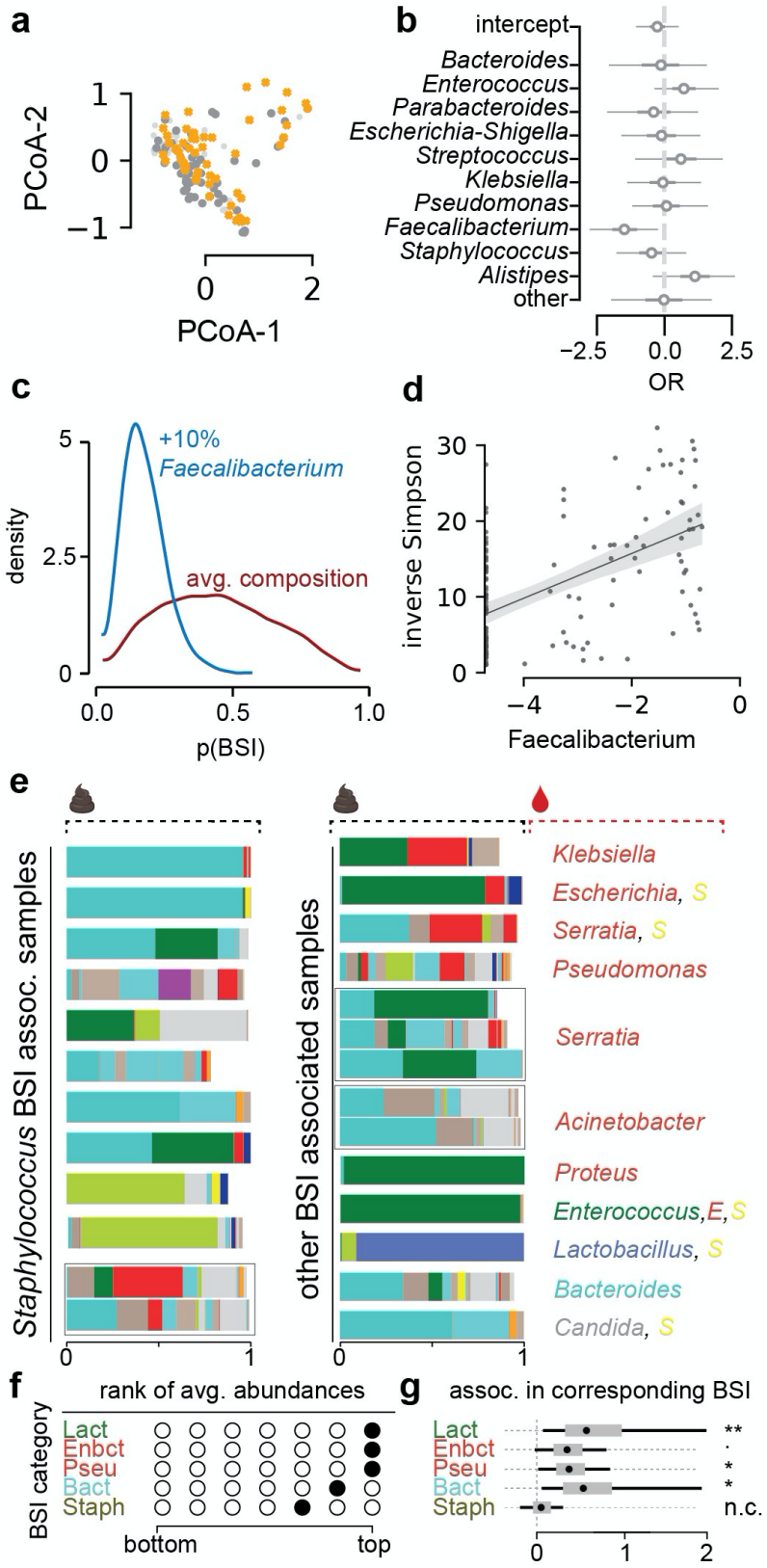
a
PCoA-2
PCoA-1
b
intercept
Bacteroides
Enterococcus
Parabacteroides
Escherichia-Shigella
Streptococcus
Klebsiella
Pseudomonas
Faecalibacterium
Staphylococcus
Alistipes
other
OR
c
+10%
Faecalibacterium
avg. composition
density
p(BSI)
d
inverse Simpson
Faecalibacterium
e
Staphylococcus BSI assoc. samples
other BSI associated samples
Klebsiella
Escherichia, S
Serratia, S
Pseudomonas
Serratia
Acinetobacter
Proteus
Enterococcus,E,S
Lactobacillus, S
Bacteroides
Candida, S
f
rank of avg. abundances
BSI category
Lact
Enbct
Pseu
Bact
Staph
bottom
top
g
assoc. in corresponding BSI
Lact
Enbct
Pseu
Bact
Staph
**
*
*
n.c.

Figure 3

461

462 **Supporting Information**

463

464 **Extended Data Figure S1. Plaque assay; SARS-CoV2 replicates in the lungs of *K18-ACE2tg* mice**
465 **infected with 10 PFU.** Lungs from mice LD3, LD4, LD5 were harvested 7 days post-infection and
466 homogenized in 500uL PBS. A lung collected 2 days post-infection from a mouse infected with 200 PFU
467 in another experiment was used as positive control (left). Viral load in the homogenates was determined
468 by plaque assay by incubation for 1h of 1/10 (top), 1/100 (middle) or 1/1000 (bottom) dilutions of the
469 homogenates on Vero E6 cells. After 1h incubation, cells were overlayed with agarose containing
470 medium. 72h post infection, the cells were fixed and stained with crystal violet. Plaques are visible as
471 holes in the stained cell layer, one plaque is counted as one viral particle present in the diluted
472 suspension.

473

474 **Extended Data Figure S2. Weight- and diversity loss during SARS-CoV-2 infection in mice. a** z-
475 scores of *α*-diversity (top) and body weight (bottom) over time; colors per mouse. **b** Difference in [g] of
476 body weight from day of infection and six days after for the different experimental groups (HD: high viral
477 dose, LD: low viral dose, CTRL: uninfected control).

478

479 **Extended Data Figure S3. Microbiome diversity is associated with clinical metadata. a-c** *α*-diversity
480 in patients with different clinical status; respectively, ICU treatment required, gastrointestinal symptoms
481 reported, positive blood culture detected (***: 99%HDI <0, **: 95%HDI <0, BEST analysis of difference in
482 means [24]). **d** Fractional overlap between clinical metadata categories in **a-c**.

483

484 **Extended Data Figure S4. Microbiome composition is associated with secondary bloodstream**
485 **infections.** All stool samples ordered by bacterial α-diversity (GMB) visualized as bars representing
486 relative bacterial genus abundances, alongside microorganisms identified in the blood (BSI) using the
487 same color scheme.

488

489 **Extended Data Figure S5. Rank abundances in uninfected samples and global GMB association**
490 **coefficients with BSIs. a** Rank of BSI predictors in the GMB of uninfected samples. **b** Posterior
491 association coefficient estimates of GMB predictors; ***: 99% HDI>0, **: 95%HDI>0, *: 90%HDI>0, .:85%
492 HDI>0.

493

494 **Extended Data Table S1. Mouse disease scores.** Scoring system: Reduced activity/resistance = 1, if
495 not moving = 2, ruffled fur=1, hatched posture = 1 or 2, heavy breathing =1

496

Extended Data Table S2. Clinical Characteristics of Patients with Confirmed COVID-19 at NYU Langone Health.

Extended Data Table S3. Clinical Characteristics of Patients with Confirmed COVID-19 at YNHH.

505 **Extended Data Figure S1**

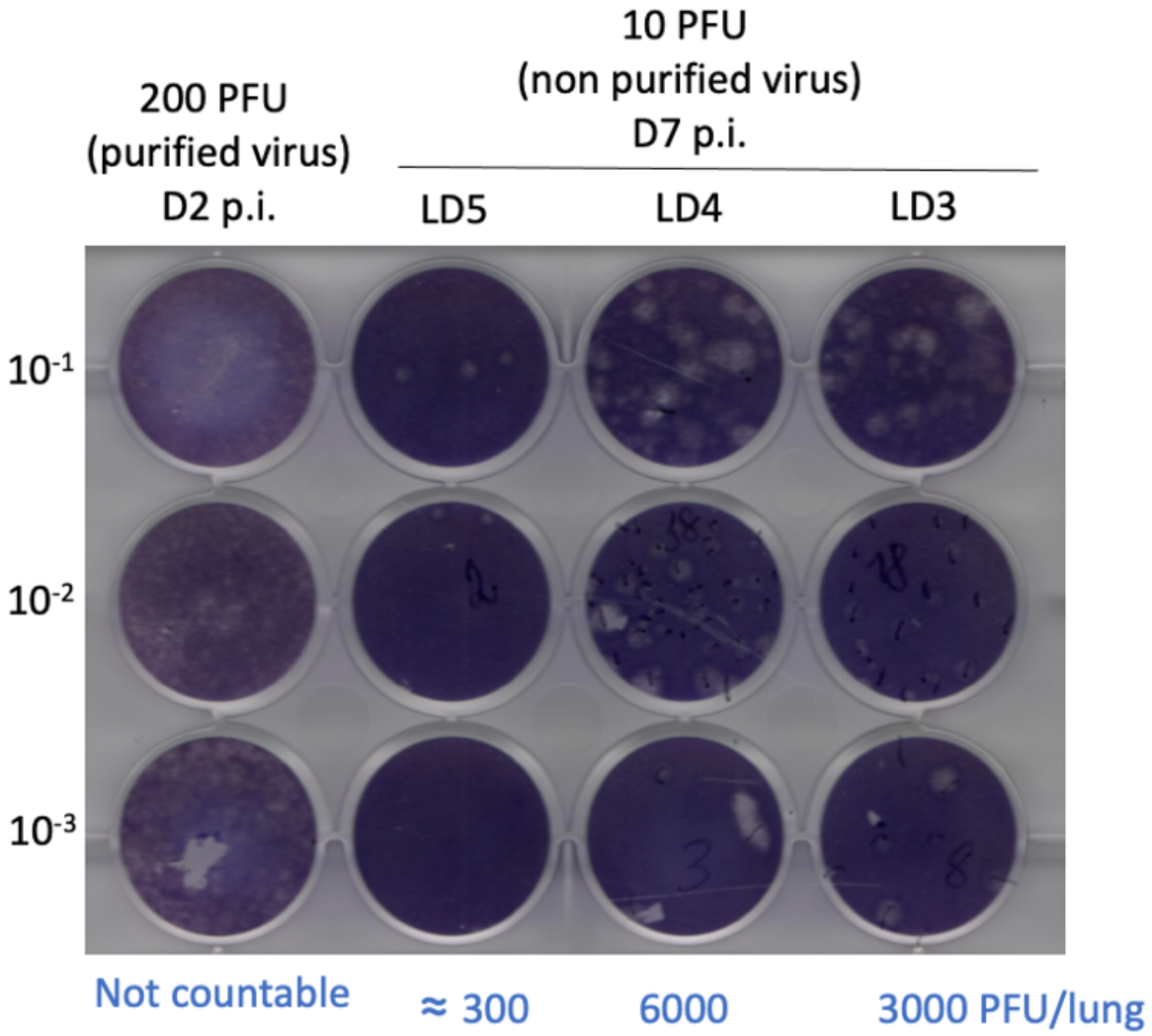

506

Extended Data Figure S2

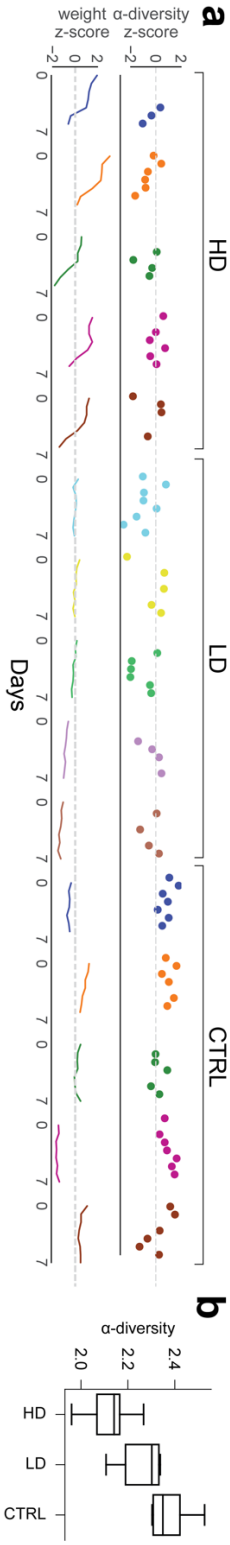

Extended Data Figure S3

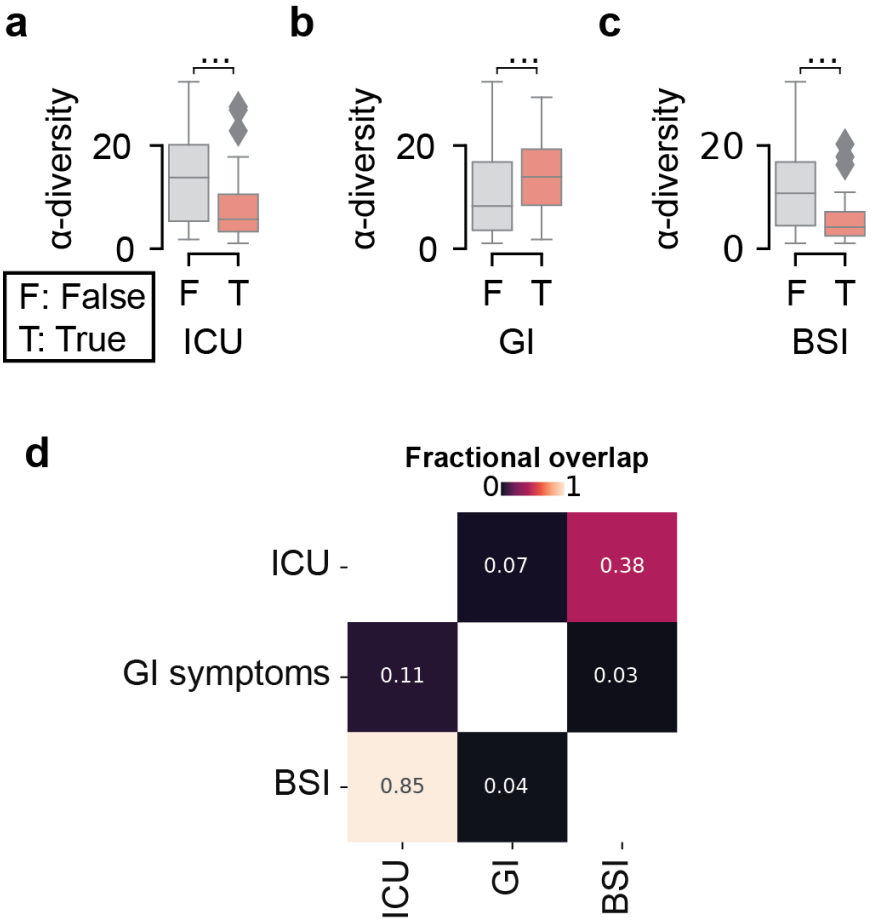

Extended Data Figure S4

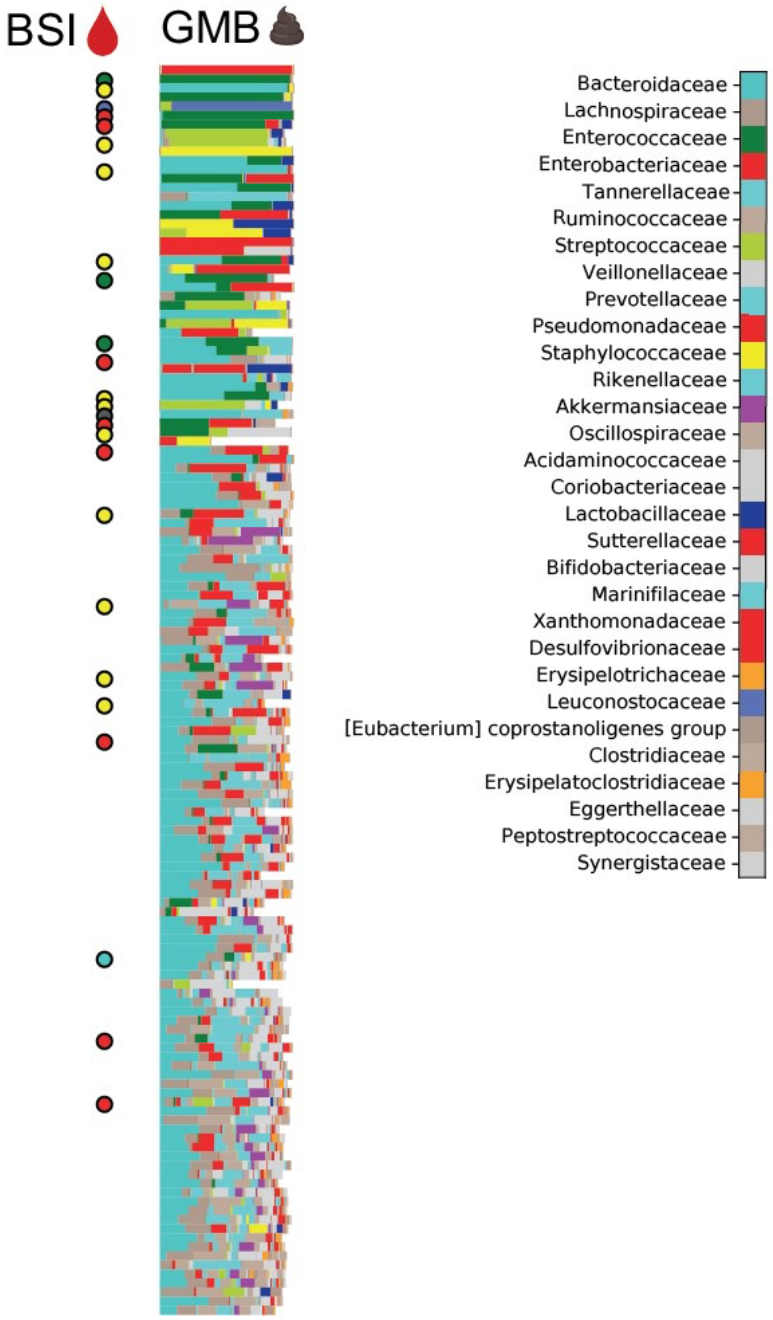

Extended Data Figure S5

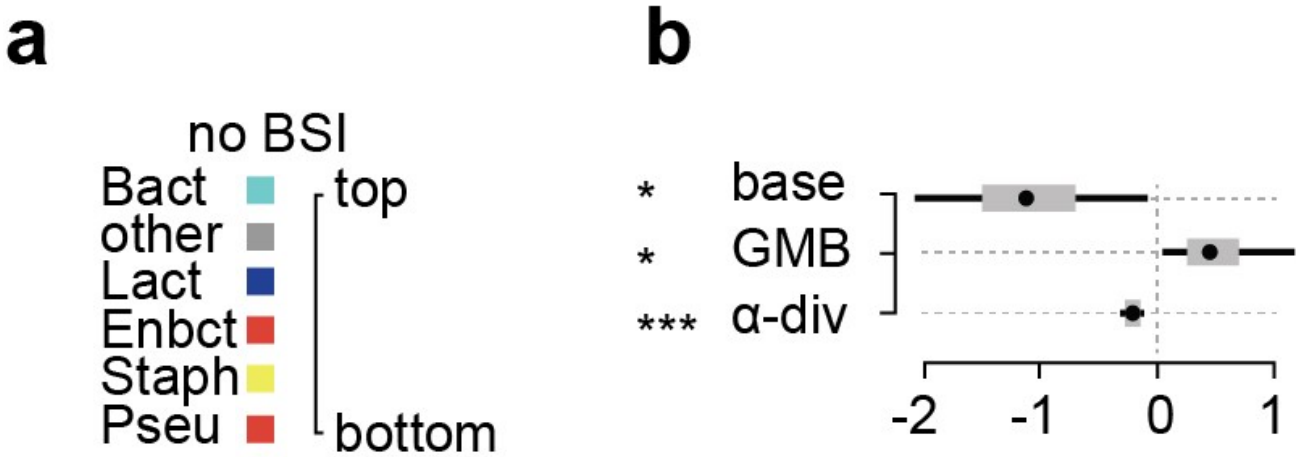

517 **Extended Data Table S2: Clinical Characteristics of Patients with Confirmed COVID-19 at NYU**
518 **Langone Health.**
519

	N=65
Age (median, IQR)	51 (31-66)
Sex	
Male	58%
Female	42%
Admission Type	
Ambulatory	17%
Hospital	83%
Comorbidities	
Hypertension	38%
Hyperlipidemia	18%
Obesity	25%
Hypothyroid	5%
Diabetes Mellitus	32%
Chronic Viral Infection (HIV/Hepatitis)	10%
COPD	7%
ESRD/CKD	7%
Current Malignancy - blood	5%
Current Malignancy - other	2%
History of DVT	3%
Organ Transplantation	10%
SLE	3%
Immunosuppression	17%
IBD	22%
Presenting Symptoms	
Fever > 99F	46%
Cough	28%
Sputum	3%
Shortness of Breath	40%
Diarrhea	45%

Hospital Course and Outcomes	
ICU Admission	53%
Pneumonia	42%
Diarrhea	13%
Intubation	36%
Sepsis	23%
Encephalopathy	12%
Death	5%
Length of Stay (days, median, IQR)	37 (10-86)
Chest Radiograph Findings	
Bilateral haziness/opacities	38%
Unilateral haziness/opacities	3%
Bilateral Effusion	5%
Unilateral Effusion	3%
Consolidation	7%
Atelectasis	3%

520
521
522 **Extended Data Table S3: Clinical Characteristics of Patients with Confirmed COVID-19 at Yale New**
523 **Haven Hospital.**

	N=37
Age (years)	62.52 ± 19.72 (n=33)
Sex (F | M)	39% | 61% (n=33)
BMI	31.22 ± 10.3 (n=25)
Race and Ethnicity	
Black or African-American	52% (n=17/33)
Hispanic or Latino	15% (n=5/33)
Asian	0% (n=0/33)
Caucasian	33% (n=11/33)
Other	0% (n=0/33)
Risk Factors	
None Admitted	16% (n=4/25)
Cancer within 1 year	4% (n=1/25)
Chronic Heart Disease	36% (n=9/25)
Hypertension	64% (n=16/25)
Chronic Lung Disease	20% (n=5/25)
Immunosupression	4% (n=1/25)

Acknowledgments

We thank René Niehus for helpful discussions on the implementation of the various Bayesian analyses.

Author contribution

LB performed the mouse experiments with help from MGN, AMVJ. MV, JEA and JS prepared the samples from NYU. MV, JEA prepared the clinical data from NYU with help from JG, EW, BS. JK provided the data from Yale with help from ACM and the IMPACT team, AIK and AI. JS designed and performed the analyses with help from GAH and APS. JS and KC designed the research question with support from VJT and BS. JS and KC wrote the manuscript. All other authors contributed materials, scientific feedback and commented on the manuscript.

Funding

This work was in part funded by NYU Grossman School of Medicine startup research funds to JS, and the Yale School of Public Health and the Beatrice Kleinberg Neuwirth Fund, as well as NIH grants to KC (DK093668, AI121244, HL123340, AI130945, AI140754, DK124336), a Faculty Scholar grant from the Howard Hughes Medical Institute (KC), Crohn's & Colitis Foundation (KC), Kenneth Rainin Foundation (KC), Judith & Stewart Colton Center of Autoimmunity (KC). Further funding was provided by grants from the NIH/NIAID to MD (R01AI143639 and R21AI139374), by Jan Vilcek/David Goldfarb Fellowship Endowment Funds to AMVJ, by The G. Harold and Leila Y. Mathers Charitable Foundation to MD, and by NYU Grossman School of Medicine Startup funds to MD and KAS, and the NYU Grossman School of Medicine COVID-19 seed research funds to VJT. MN was supported by the American Heart Association Postdoctoral Fellowship 19-A0-00-1003686. IMPACT received support from the Yale COVID-19 Research Resource Fund. AI and DRL are Investigators of the Howard Hughes Medical Institute. AIK received support from the Beatrice Kleinberg Neuwirth Fund, Bristol Meyers Squibb Foundation and COVID-19 research funds from the Yale Schools of Public Health and Medicine.

Conflicts

KC has received research support from Pfizer, Takeda, Pacific Biosciences, Genentech, and Abbvie; consulted for or received an honoraria from Puretech Health, Genentech, and Abbvie; and holds U.S. patent 10,722,600 and provisional patents 62/935,035 and 63/157,225. JS is cofounder of Postbiotics Plus Research LLC.

Bibliography

1. Fajgenbaum, D. C. & June, C. H. Cytokine Storm. *N. Engl. J. Med.* **383,** 2255–2273 (2020).
2. Lucas, C. *et al.* Longitudinal analyses reveal immunological misfiring in severe COVID-19. *Nature* **584,** 463–469 (2020).
3. Zuo, T. *et al.* Alterations in Gut Microbiota of Patients With COVID-19 During Time of Hospitalization. *Gastroenterology* **159,** 944–955.e8 (2020).
4. Yeoh, Y. K. *et al.* Gut microbiota composition reflects disease severity and dysfunctional immune responses in patients with COVID-19. *Gut* **70,** 698–706 (2021).
5. Nori, P. *et al.* Bacterial and fungal coinfections in COVID-19 patients hospitalized during the New York City pandemic surge. *Infect. Control Hosp. Epidemiol.* **42,** 84–88 (2021).
6. Grasselli, G. *et al.* Hospital-Acquired Infections in Critically Ill Patients With COVID-19. *Chest* (2021). doi:10.1016/j.chest.2021.04.002
7. Langford, B. J. *et al.* Bacterial co-infection and secondary infection in patients with COVID-19: a living rapid review and meta-analysis. *Clin. Microbiol. Infect.* **26,** 1622–1629 (2020).
8. Buffie, C. G. *et al.* Precision microbiome reconstitution restores bile acid mediated resistance to Clostridium difficile. *Nature* **517,** 205–208 (2015).
9. Buffie, C. G. & Pamer, E. G. Microbiota-mediated colonization resistance against intestinal pathogens. *Nat. Rev. Immunol.* **13,** 790–801 (2013).
10. Modi, S. R., Collins, J. J. & Relman, D. A. Antibiotics and the gut microbiota. *J. Clin. Invest.* **124,** 4212–4218 (2014).
11. Morjaria, S. *et al.* Antibiotic-Induced Shifts in Fecal Microbiota Density and Composition during Hematopoietic Stem Cell Transplantation. *Infect. Immun.* **87,** (2019).
12. Niehus, R. *et al.* Quantifying antibiotic impact on within-patient dynamics of extended-spectrum beta-lactamase resistance. *Elife* **9,** (2020).
13. Taur, Y. *et al.* Intestinal domination and the risk of bacteremia in patients undergoing allogeneic hematopoietic stem cell transplantation. *Clin. Infect. Dis.* **55,** 905–914 (2012).
14. Taur, Y. *et al.* Reconstitution of the gut microbiota of antibiotic-treated patients by autologous fecal microbiota transplant. *Sci. Transl. Med.* **10,** (2018).
15. Liao, C. *et al.* Compilation of longitudinal microbiota data and hospitalome from hematopoietic cell transplantation patients. *Sci. Data* **8,** 71 (2021).
16. Peled, J. U. *et al.* Microbiota as Predictor of Mortality in Allogeneic Hematopoietic-Cell Transplantation. *N. Engl. J. Med.* **382,** 822–834 (2020).
17. Yu, D. *et al.* Low prevalence of bloodstream infection and high blood culture contamination rates in patients with COVID-19. *PLoS One* **15,** e0242533 (2020).
18. Wang, D. *et al.* Clinical Characteristics of 138 Hospitalized Patients With 2019 Novel Coronavirus-Infected Pneumonia in Wuhan, China. *JAMA* **323,** 1061–1069 (2020).
19. Westblade, L. F., Simon, M. S. & Satlin, M. J. Bacterial coinfections in coronavirus disease 2019. *Trends Microbiol.* (2021). doi:10.1016/j.tim.2021.03.018
20. Sepulveda, J. *et al.* Bacteremia and Blood Culture Utilization during COVID-19 Surge in New York City. *J. Clin. Microbiol.* **58,** (2020).
21. Lansbury, L., Lim, B., Baskaran, V. & Lim, W. S. Co-infections in people with COVID-19: a systematic review and meta-analysis. *J. Infect.* **81,** 266–275 (2020).
22. Sieswerda, E. *et al.* Recommendations for antibacterial therapy in adults with COVID-19 - an evidence based guideline. *Clin. Microbiol. Infect.* **27,** 61–66 (2021).
23. Zhai, B. *et al.* High-resolution mycobiota analysis reveals dynamic intestinal translocation preceding invasive candidiasis. *Nat. Med.* **26,** 59–64 (2020).
24. Haak, B. W. *et al.* Impact of gut colonization with butyrate-producing microbiota on respiratory viral infection following allo-HCT. *Blood* **131,** 2978–2986 (2018).
25. Steed, A. L. *et al.* The microbial metabolite desaminotyrosine protects from influenza through type I interferon. *Science* **357,** 498–502 (2017).
26. Abt, M. C. *et al.* Commensal bacteria calibrate the activation threshold of innate antiviral immunity. *Immunity* **37,** 158–170 (2012).
27. Ichinohe, T. *et al.* Microbiota regulates immune defense against respiratory tract influenza A virus infection. *Proc. Natl. Acad. Sci. USA* **108,** 5354–5359 (2011).

611 28. Sencio, V. *et al.* Influenza infection impairs the gut's barrier properties and favors secondary enteric
612 bacterial infection through reduced production of short-chain fatty acids. *Infect. Immun.* (2021).
613 doi:10.1128/IAI.00734-20
614 29. Wang, J. *et al.* Respiratory influenza virus infection induces intestinal immune injury via microbiota-
615 mediated Th17 cell-dependent inflammation. *J. Exp. Med.* **211,** 2397–2410 (2014).
616 30. Schluter, J. *et al.* The gut microbiota is associated with immune cell dynamics in humans. *Nature*
617 **588,** 303–307 (2020).
618 31. Gopalakrishnan, V. *et al.* Gut microbiome modulates response to anti-PD-1 immunotherapy in
619 melanoma patients. *Science* **359,** 97–103 (2018).
620 32. Diefenbach, C. S. *et al.* Microbial dysbiosis is associated with aggressive histology and adverse
621 clinical outcome in B-cell non-Hodgkin lymphoma. *Blood Adv.* **5,** 1194–1198 (2021).
622 33. Sokol, H. *et al.* Faecalibacterium prausnitzii is an anti-inflammatory commensal bacterium identified
623 by gut microbiota analysis of Crohn disease patients. *Proc. Natl. Acad. Sci. USA* **105,** 16731–16736
624 (2008).
625 34. Wrzosek, L. *et al.* Bacteroides thetaiotaomicron and Faecalibacterium prausnitzii influence the
626 production of mucus glycans and the development of goblet cells in the colonic epithelium of a
627 gnotobiotic model rodent. *BMC Biol.* **11,** 61 (2013).
628 35. Gaebler, C. *et al.* Evolution of antibody immunity to SARS-CoV-2. *Nature* **591,** 639–644 (2021).
629 36. Park, S.-K. *et al.* Detection of SARS-CoV-2 in Fecal Samples From Patients With Asymptomatic and
630 Mild COVID-19 in Korea. *Clin. Gastroenterol. Hepatol.* **19,** 1387–1394.e2 (2021).
631 37. Xiao, F. *et al.* Evidence for Gastrointestinal Infection of SARS-CoV-2. *Gastroenterology* **158,** 1831–
632 1833.e3 (2020).
633 38. Cheung, K. S. *et al.* Gastrointestinal Manifestations of SARS-CoV-2 Infection and Virus Load in
634 Fecal Samples From a Hong Kong Cohort: Systematic Review and Meta-analysis. *Gastroenterology*
635 **159,** 81–95 (2020).
636 39. Lamers, M. M. *et al.* SARS-CoV-2 productively infects human gut enterocytes. *Science* **369,** 50–54
637 (2020).
638 40. Wang, L. *et al.* An observational cohort study of bacterial co-infection and implications for empirical
639 antibiotic therapy in patients presenting with COVID-19 to hospitals in North West London. *J.*
640 *Antimicrob. Chemother.* **76,** 796–803 (2021).
641 41. Matsuzawa-Ishimoto, Y. *et al.* Autophagy protein ATG16L1 prevents necroptosis in the intestinal
642 epithelium. *J. Exp. Med.* **214,** 3687–3705 (2017).
643 42. Labarta-Bajo, L. *et al.* Type I IFNs and CD8 T cells increase intestinal barrier permeability after
644 chronic viral infection. *J. Exp. Med.* **217,** (2020).
645 43. Karki, R. *et al.* Synergism of TNF-α and IFN-γ Triggers Inflammatory Cell Death, Tissue Damage,
646 and Mortality in SARS-CoV-2 Infection and Cytokine Shock Syndromes. *Cell* **184,** 149–168.e17
647 (2021).
648 44. Gohl, D. M. *et al.* Systematic improvement of amplicon marker gene methods for increased accuracy
649 in microbiome studies. *Nat. Biotechnol.* **34,** 942–949 (2016).
650 45. Wang, Q., Garrity, G. M., Tiedje, J. M. & Cole, J. R. Naive Bayesian classifier for rapid assignment of
651 rRNA sequences into the new bacterial taxonomy. *Appl. Environ. Microbiol.* **73,** 5261–5267 (2007).
652 46. Pawlowsky-Glahn, V., Egozcue, J. J. & Tolosana-Delgado, R. *Modelling and analysis of*
653 *compositional data*. (John Wiley & Sons, Ltd, 2015). doi:10.1002/9781119003144
654 47. Kruschke, J. K. Bayesian estimation supersedes the t test. *J. Exp. Psychol. Gen.* **142,** 573–603
655 (2013).
656 48. Homan, M. D. & Gelman, A. The No-U-Turn Sampler: Adaptively Setting Path Lengths in
657 Hamiltonian Monte Carlo. *J. Mach. Learn. Res.* **15,** 1593–1623 (2014).
658